

Localization of the Counterion of the Protonated Schiff Base of *n*-butylretinal in Solution[†]

Nikola Biliškov,^a Jurica Novak,^a Milena Petković,^b Goran Zgrablić,^c
 Goran Baranović,^a and Nada Došlić^{a,*}

^a*Ruđer Bošković Institute, Bijenička 54, 10000 Zagreb, Croatia*

^b*Faculty of Physical Chemistry, University of Belgrade, Studentski trg, 12–16, 11000 Belgrade, Serbia*

^c*Sincrotrone Trieste, S.S. 14 km 163.5 in Area Science Park, 34012 Basovizza Trieste, Italy*

RECEIVED FEBRUARY 1, 2011; REVISED MARCH 30, 2011; ACCEPTED APRIL 28, 2011

Abstract. The vibrational spectra of the protonated Schiff base of *n*-butylretinal (*n*SBR⁺) in dichloromethane are studied. The trifluoroacetic acid (TFA) is used for the protonation of the Schiff base of *n*-butylretinal (*n*SBR). Combining the two-dimensional correlation analysis of the experimental infrared spectra with anharmonic frequency calculations it is shown that two types of ionic aggregates between *n*SBR⁺ and the TFA counterion are formed.

The study suggests that the interaction between *n*SBR⁺ and the TFA counterion may be responsible for the observed loss of photoselectivity in the *trans-cis* isomerization of the *n*SBR⁺ in solution. (doi: 10.5562/cca1826)

Keywords: *n*-butylretinal; trifluoroacetic acid; infrared spectroscopy; hydrogen bonding; DFT; anharmonic frequency

INTRODUCTION

The photoinduced *trans-cis* isomerization of the protonated Schiff base of retinal, the photosensitive chromophore in retinal proteins, has been the subject of numerous experimental and theoretical investigations for many years.^{1–16} In the protein environment the photoisomerization reaction takes place on the time scale of ≤ 400 fs,¹⁷ occurs selectively around the C₁₃=C₁₄ double bond and leads to the 13-*cis* product with a quantum yield of more than 60%.⁹ This high efficiency of photoisomerization is the key of the biological activity of retinal proteins.^{13,18}

In solution the photoselectivity is lost,^{19–21} but the all-*trans* to 11-*cis* isomerization is the most efficient reaction path. The reaction proceeds on the time scale of picoseconds and the excited state lifetime has multiexponential decay pointing to multiple emitting species.²² Interestingly, the femtosecond fluorescence spectroscopy experiments of Zgrablić *et al.* have shown that the excited state lifetime of the protonated *n*-butylamine Schiff base of retinal (*n*SBR⁺) is almost unaffected by the properties of the solvents.²² As the trifluoroacetic acid (TFA) was used for protonation of the retinal Schiff base this suggests that the formation of an ionic complex between *n*SBR⁺ and the TFA counterion can

be responsible for the loss of photoselectivity in solution. Despite of the fundamental and technological relevance of the reaction, information on intermolecular interactions between the chromophore, the counterion and the solvent is relatively scarce.^{23–27} Thus the goal of this investigation is to shed light on these interactions.

Vibrational spectroscopy is the method of choice for investigating hydrogen bond interactions and structural changes.^{28–32} The formation of a hydrogen bond induces couplings between normal modes of the monomers that leads to the characteristic broadening and downshift of the hydrogen-donor stretching vibration.^{29,33} In the system at hand, however, the highly informative $\nu(\text{N-H}^+)$ stretching vibration expected in the 2900–2800 cm⁻¹ region is overlapped by solvent absorption and the numerous CH stretching bands that congest the spectrum. In order to assign the rather complex spectrum arising from the binding of TFA to *n*SBR, we use 2D IR correlation spectroscopy. Apart from facilitating the assignment by spreading the spectrum in two dimensions, 2D IR correlation spectroscopy provides information on the order of the spectral intensity changes taking place during a series of concentration measurement.³⁴ Furthermore, to unravel the intermolecular interactions involving *n*SBR⁺, we focus on the less anharmonic $\delta(\text{NH}^+)$ bending and $\nu(\text{C=N}^+)$

[†] This article belongs to the Special Issue *Chemistry of Living Systems* devoted to the intersection of chemistry with life.

* Author to whom correspondence should be addressed. (E-mail: nadja.doslic@irb.hr)

stretching vibrations. The experiments of Zgrablić *et al.*²² were performed in 3-5 fold excess of TFA. In such circumstances one expects the formation of either open or cyclic TFA dimers characterized by a broad and downshifted $\nu(\text{OH}\cdots\text{O})$ stretching vibration.³⁵ The strength of the OH \cdots O hydrogen bond between the two TFA units will be affected by the assembly with *n*SBR⁺.³⁶ Hence the downshift of the $\nu(\text{OH}\cdots\text{O})$ stretching vibration of the TFA dimer is a marker for the formation of a hydrogen bonded association with *n*SBR⁺. In order to uncover these interactions it seems desirable to support the experimental assignment by quantum chemical calculations of anharmonic frequencies.³⁷⁻³⁹

The rest of the paper is organized as follows. In the next section we outline the experimental and theoretical approach. In Section 3 the results are presented. Specifically, a step by step comparison between experiment and theory that leads to identification of the species present in the experiments will be presented. The paper is concluded in Section 4.

EXPERIMENTAL AND THEORETICAL METHODS

IR spectroscopy

The *n*-butylamine Schiff base (*n*SBR) was prepared as described previously²² and dissolved in dichloromethane ($c(\text{nSBR}) = 1.06 \text{ mmol dm}^{-3}$). Trifluoroacetic acid (TFA) of spectrophotometric grade (> 99 % pure) was used for protonation. In total 21 samples were prepared in the concentration range $c(\text{TFA}) = 0\text{--}2.03 \text{ mmol dm}^{-3}$, corresponding to $c(\text{TFA})/c(\text{nSBR})$ molar ratio from 0 to 2. No self aggregation of the *n*SBR occurs in the concentration range chosen for the measurements.

The infrared spectra were obtained with the ABB Bomem MB102 Fourier-transform infrared spectrometer with a DTGS detector and CsI optics. The transmission technique was used to record the spectra. Since the model MB102 is a single-beam spectrometer, a background was taken before measuring each sample. The use of CaF₂ windows restricted the spectral range to 4000 – 1000 cm⁻¹. Each spectrum represents an average of 10 Fourier-transformed interferograms. The nominal resolution was 2 cm⁻¹, which gives a distance between two points in the resulting spectrum $\Delta\tilde{\nu} = 0.97 \text{ cm}^{-1}$. The thickness of the transmission cells was determined using dichloromethane as secondary standard for calibration.⁴⁰

The spectrum of pure dichloromethane was subtracted from all spectra of solutions. The spectra were normalized to the total concentration of *n*SBR and corrected for the baseline by subtraction of the line defined by two utmost points in the considered spectral range. Since hydrogen bonding often leads to inhomogeneous

line broadening the spectral features of interest were fitted to the general Voigt line profile. The convolution integral was computed by the IgorPro data analysis program.⁴¹

Dynamic spectra, showing the intensity variations at wavenumbers ν_1 and ν_2 as function of the concentration ratio $c(\text{TFA})/c(\text{nSBR})$, were obtained by subtracting the first spectrum, *i.e.*, the *n*SBR spectrum, from the remaining 20 spectra of the *n*SBR + TFA series. The intensity of the 2D correlation spectrum³⁴

$$X(\nu_1, \nu_2) = \Phi(\nu_1, \nu_2) + i \Psi(\nu_1, \nu_2)$$

comprises a synchronous $\Phi(\nu_1, \nu_2)$ and an asynchronous $\Psi(\nu_1, \nu_2)$ component. The intensity of a synchronous 2D correlation peak $\Phi(\nu_1, \nu_2)$ represents simultaneous or coincidental changes of two intensity variations measured at two wavenumbers ν_1 and ν_2 . In contrast, the intensity of the asynchronous spectrum $\Psi(\nu_1, \nu_2)$ represents sequential or successive changes of two intensity variations measured at the two wavenumbers ν_1 and ν_2 . Consequently, the asynchronous spectrum consists of cross peaks only and they appear only if the intensities of the two spectral changes do not coincide. The evolving factor analysis, used to determine the number of interacting species in the sample⁴² has been performed with the Specfit v.2.11 programme.⁴³

Electronic structure and bound state computations

All quantum mechanical calculations have been performed with the Gaussian 09 suit of programs.⁴⁴ Geometry optimizations and vibrational frequency calculations of *n*SBR and the complexes formed with one and two TFA units were carried out with the hybrid B3LYP density functional⁴⁵ with the TZVP basis set.⁴⁶ The effect of the solvent, dichloromethane, has been taken into account via the polarization continuum model as implemented in Gaussian 09. The default value of the dielectric constant of $\epsilon = 8.93$ has been used. In other words we have assumed that the solvent dynamics is much slower than the investigated N–H and O–H bending and stretching motions.

In hydrogen-bonded systems the anharmonicity of the bending vibrations is small and their frequencies are upshifted with respect to the harmonic values. On the contrary, the stretching vibrations are downshifted and their harmonic frequencies are often scaled to easy the comparison with experiment. Here we use a scaling factor of 0.978 adequate for the B3LYP functional and a basis set of triple zeta valence quality. However the frequency of the hydrogen-donor stretching vibration is significantly downshifted and anharmonic frequency calculations are needed to simulate the spectra.^{33,38} The size of the systems at hand encompassing up to 228

normal modes precludes the calculation of the full dimensional anharmonic force field.

Hence we compute the anharmonic IR spectra of the hydrogen-donor stretching vibration in reduced dimensionality using the normal mode representation of the Hamiltonian

$$H = \sum_i \frac{P_i^2}{2m_i} + V(\mathbf{Q}) \quad (1)$$

where $\{Q_i\} = \mathbf{Q}$ is the set of normal modes that span the potential energy surface (PES) and m_i are the corresponding effective masses as given by Gaussian 09. The remaining normal modes were kept frozen. In order to identify the normal modes that couple strongly to the hydrogen-donor stretching vibration we computed all cubic and semidiagonal quartic force constants that contain this mode. The anharmonic force constants K_{ijk} and K_{ijkl} , with i denoting the hydrogen-donor stretch, were determined numerically by calculating the first and the second derivatives of analytical quadratic force constants K_{ij} , using the five-point difference procedure.^{47,48} One- to four-dimensional (1D-4D) calculations were performed to obtain the anharmonic frequencies of the normal modes of interest. The time-independent Schrödinger equation was solved using the Fourier grid Hamiltonian method,^{49,50} while the implicitly restarted Lanczos method was used for the diagonalization of the Hamiltonian matrix.⁵¹ The assignment of the eigenstates of the 4D model Hamiltonian was performed by projection on the zero-order states of the uncoupled Hamiltonian.

RESULTS AND DISCUSSION

In the following we denote the neutral form of the Schiff base of *n*-butyl retinal by *n*SBR, while *n*SBR⁺ denotes its protonated form. The latter is often denoted by PSBR in the literature. The *n*SBR molecule contains a characteristic imine C=N group with a lone electron pair located at the nitrogen, making it a strong organic Schiff base with $pK_B = 10.75$.⁵² The imine group acts as the hydrogen bond accepting site. On the other hand, TFA is a strong organic acid with $pK_A = 0.52$ (Ref. 53) and its OH group serves as a proton donor.

Due to the relative strength of both acid and base, it is expected that the hydrogen bonding interaction of the acid – base pair, C=N---H–O, causes the protonation of the N atom of *n*SBR through the equilibrium



giving rise to an ionic pair $[n\text{SBR}^+ \text{TFA}^-]$. The protonated form, *n*SBR⁺, is characterized by $pK_A = 5.99$.

The evolving factor analysis was used to elucidate the number of species present in the system. It was found that three species define the system while all other factors were under the level of experimental error and thus represented noise. We assume that the first two species are *n*SBR and $[n\text{SBR}^+ \text{TFA}^-]$. The existence of the third species can be interpreted either as a dimer of TFA or as $[n\text{SBR}^+ \text{TFA}^-]\text{TFA}$.

TFA dimers have a characteristic spectrum featuring a complex carbonyl absorption in the 1900–1700 cm^{-1} region and a broad absorption around 3100 cm^{-1} , assigned to the asymmetric $\nu(\text{OH})$ of the 8-membered carboxyl ring.^{35,54} Shipman *et al.*³⁵ have recorded the spectra of the TFA monomers and dimers in CCl_4 and assigned the higher frequency band at 1825 cm^{-1} to the carboxyl stretching of the monomer, and the one at 1775 cm^{-1} to the carboxyl stretching of the dimer. We recorded the spectra of TFA in dichloromethane, in the concentration range 1–50 mmol dm^{-3} and compared them to the ones observed for the TFA – *n*SBR system. For TFA in dichloromethane the carboxyl stretching band consists of two components, a strong band at 1804 cm^{-1} , and a weaker one at 1783 cm^{-1} . On the contrary, in TFA

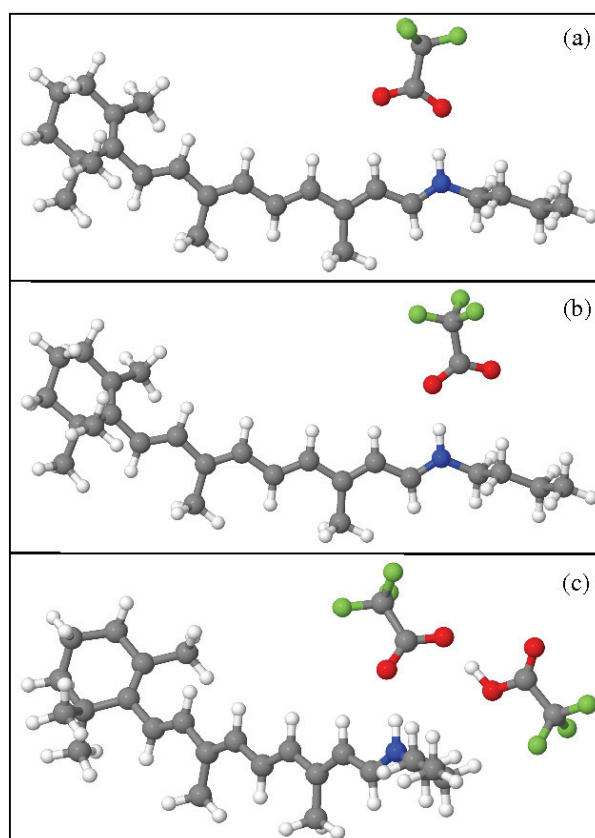


Figure 1. The minimum energy structure of $[n\text{SBR}^+ \text{TFA}^-]$ (a), the structure of a local minimum of $[n\text{SBR}^+ \text{TFA}^-]$ $E = 0.41$ kcal/mol above in energy (b) and the minimum energy structure of $[n\text{SBR}^+ \text{TFA}^-]\text{TFA}$ (c) as computed at the B3LYP/TZVP level.

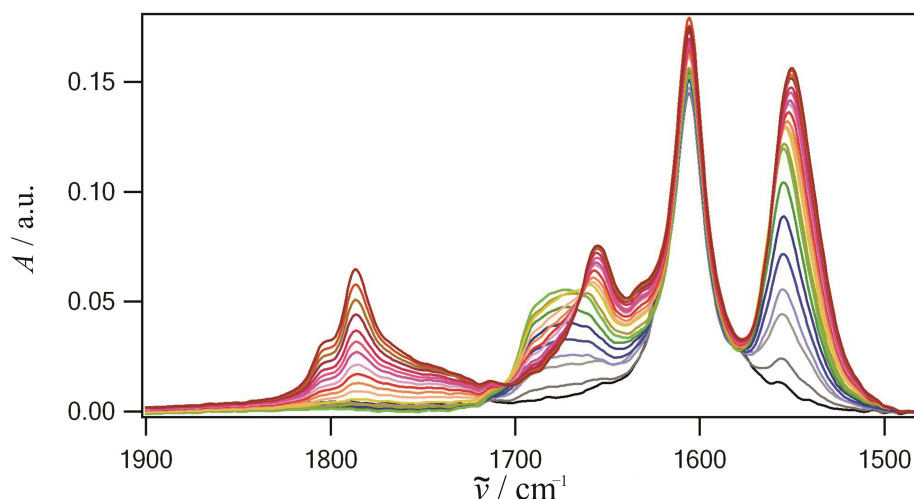


Figure 2. Infrared spectra of titration of *n*SBR with TFA in the 1900 – 1480 cm^{-1} region. The concentration range is $0 < c(\text{TFA})/c(n\text{SBR}) < 2$. The strongest band at 1796 cm^{-1} corresponds to the highest ratio of $c(\text{TFA})/c(n\text{SBR})$.

– *n*SBR the first band is observed at the same position as a weak shoulder, whereas the second band is found at 1786 cm^{-1} . The change in the relative intensity of the two bands indicates a strong interaction of *n*SBR with the TFA that modifies the monomer-dimer dynamics of TFA in dichloromethane. To investigate these findings in more detail we recorded the IR spectra of titration of *n*SBR with TFA in the concentration range $0 < c(\text{TFA})/c(n\text{SBR}) < 2$. Figure 2 reports the resulting spectra. Focusing on the region between 1750 and 1810 cm^{-1} one readily observes a broad band with a strong increase of intensity as a function of TFA concentration. The gain in intensity is a characteristic feature of strongly downshifted OH stretching vibrations. Thus, in our opinion, the carboxyl and hydroxyl stretching bands of $[\text{nSBR}^+ \text{TFA}^-]\text{TFA}$ overlap in the 1750–1810 cm^{-1} spectral region. We will shortly support this assignment by multidimensional eigenstates calculation including both, the C=O and O–H stretching vibrations.

The structures of both hydrogen bonded compounds, $[\text{nSBR}^+ \text{TFA}^-]$ and $[\text{nSBR}^+ \text{TFA}^-]\text{TFA}$, as computed on the B3LYP/TZVP level of theory are shown in Figure 1. Because of the single hydrogen bond, the $[\text{nSBR}^+ \text{TFA}^-]$ complex is quite fluxional.⁵⁵ As a matter of fact apart from the global minimum shown in Figure 1a, a local minimum structure in which the COO^- group of TFA^- is rotated by 180° toward the *n*-butyl part of the molecule has been located 0.41 kcal/mol above in energy (Figure 1b). In case of $[\text{nSBR}^+ \text{TFA}^-]\text{TFA}$, the second TFA molecule is bonded *via* O–H---O=C type hydrogen bond to the TFA^- counterion that directly interacts with the NH^+ group of *n*SBR⁺. At the B3LYP/TZVP level of calculation this leads to the prolongation of the (N–O) distance from 2.73 Å in $[\text{nSBR}^+ \text{TFA}^-]$ to 2.81 Å in $[\text{nSBR}^+$

$\text{TFA}^-]\text{TFA}$. In other words the formation of $[\text{nSBR}^+ \text{TFA}^-]\text{TFA}$ weakens the $\text{N}^+ \text{---} \text{H} \text{---} \text{O}$ hydrogen bond.

Let us recall that in the IR spectra, the formation of $[\text{nSBR}^+ \text{TFA}^-]$ should be reflected mainly in the occurrences of the $\delta(\text{NH}^+)$ bending at around 1550 cm^{-1} and of the shifted $\nu(\text{C}=\text{N})$ stretching vibrations of *n*SBR⁺ from 1680 cm^{-1} to 1650 cm^{-1} . Namely, if protonation occurs, it gives rise to new normal modes due to the formation of NH^+ group, *i.e.* $\nu(\text{NH}^+)$ and $\delta(\text{NH}^+)$. However, the $\nu(\text{NH}^+)$ region is highly obscured by very complex absorption in 3000–2700 cm^{-1} region and cannot be used for the assignment. The formation of $[\text{nSBR}^+ \text{TFA}^-]\text{TFA}$ can be monitored through the change in absorption of the $\nu(\text{OH} \text{---} \text{O})$ stretching vibration.

Titration of *n*SBR with TFA

The 1D IR spectra of titration of *n*SBR with TFA in the spectral range between 1900 and 1480 cm^{-1} are shown in Figure 2. Three bands centered at around 1550, 1660 and 1790 cm^{-1} display a strong dependence of the intensity on the TFA concentration. Although there is no solvent absorption in the 1900–1480 cm^{-1} range, the richness of spectral features makes it hard to resolve from one-dimensional spectra. Thus the 2D correlation maps of $\Phi(\nu_1, \nu_2)$ and $\Psi(\nu_1, \nu_2)$ shown in the left and right panels of Figure 3, respectively, were used to facilitate the analysis. The synchronous spectrum of $0 < c(\text{TFA})/c(n\text{SBR}) < 2$ (Figure 3, top, left) is dominated by three autopeaks at 1551, 1658 and 1786 cm^{-1} . To resolve the spectral changes due to the formation of $[\text{nSBR}^+ \text{TFA}^-]$ and $[\text{nSBR}^+ \text{TFA}^-]\text{TFA}$, the 2D correlation maps for the molar ratio $0 < c(\text{TFA})/c(n\text{SBR}) < 1$ and $1 < c(\text{TFA})/c(n\text{SBR}) < 2$ are shown in the middle and bottom panels of Figure 3, respectively. The positive sign of the

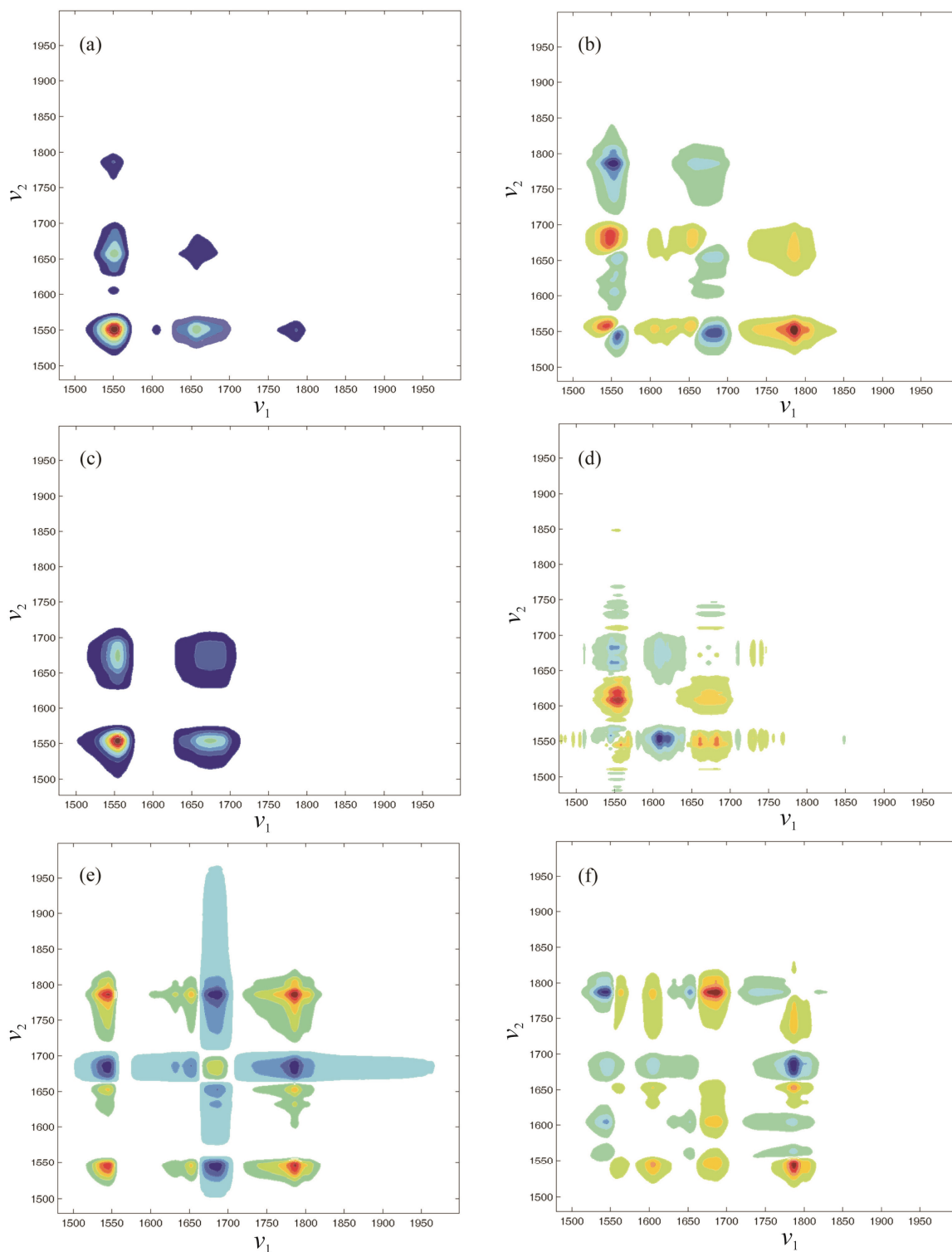


Figure 3. 2D IR correlation maps for titration of *n*SBR with TFA: (a), (c) and (e) synchronous $\Phi(\nu_1, \nu_2)$ maps; (b), (d) and (f) asynchronous $\Psi(\nu_1, \nu_2)$ maps; (a) and (b) $0 < c(\text{TFA})/c(n\text{SBR}) < 2$; (c) and (d) $0 < c(\text{TFA})/c(n\text{SBR}) < 1$; (e) and (f) $1 < c(\text{TFA})/c(n\text{SBR}) < 2$.

cross peaks reflects the increase in intensity of the considered bands due to the aggregation of *n*SBR with TFA. From the synchronous maps it is evident that the major

changes occur in the region around 1550 cm^{-1} and 1675 cm^{-1} due to the formation of $[n\text{SBR}^+ \text{TFA}^-]$, while the formation of $[n\text{SBR}^+ \text{TFA}^-]\text{TFA}$ is reflected in the

1652 cm^{-1} band and in the region around 1780 cm^{-1} . In the asynchronous maps for $0 < c(\text{TFA})/c(n\text{SBR}) < 2$, two bands are found at 1550 cm^{-1} and three not well resolved bands are found at 1780 cm^{-1} .

(a) 1620–1550 cm^{-1} region

We first consider the region of absorption centered at 1550 cm^{-1} (Figure 2). This absorption is almost totally absent in the spectrum of *n*SBR. For $c(\text{TFA})/c(n\text{SBR}) < 1$ it shows a rapid increase of intensity, but for $c(\text{TFA})/c(n\text{SBR}) > 1$ the increase is slower. The 2D IR asynchronous correlation shows that this region consists of at least four bands, located at 1567, 1559, 1545 and 1533 cm^{-1} that are not well resolved in the 1D spectra. All four bands are interpreted as the bending vibrations of the NH^+ oscillator due to the protonation of *n*SBR by TFA in both $[\text{nSBR}^+ \text{TFA}^-]$ and $[\text{nSBR}^+ \text{TFA}^-]\text{TFA}$. This assignment is supported by B3LYP/TZVP calculation. The observed and computed frequencies are compared in Table 1. Two normal modes with large contribution of the NH^+ bending vibration denoted, $\delta(\text{NH}^+)$ and $\delta(\text{NH}^+) + \delta(\text{CH})$ are found for each conformer. They are intercalated by the strong $\nu(\text{C}=\text{C})$ skeletal stretching vibration. It is apparent that the experimental and theoretical assignments at 1563 cm^{-1} and 1608 cm^{-1} are reversed. In our opinion the disagreement can be attributed to the coupling of normal modes and the intensity borrowing mechanism that cannot be accounted for in the harmonic approximation. Moreover, the spectra shown in Figure 2 reveal that neither the position nor the intensity of the band at 1608 cm^{-1} are sensitive to the addition of TFA. Thus in agreement with Smith *et al.*⁵⁶ and the computed $\nu(\text{C}=\text{C})$ frequency of *n*SBR we assign the band to the stretching of the $\text{C}=\text{C}$ bonds of retinal.

(b) 1700–1640 cm^{-1} region

Next we focus on the complex absorption envelope in the 1700–1640 cm^{-1} region. According to Gilson *et al.*⁵⁷

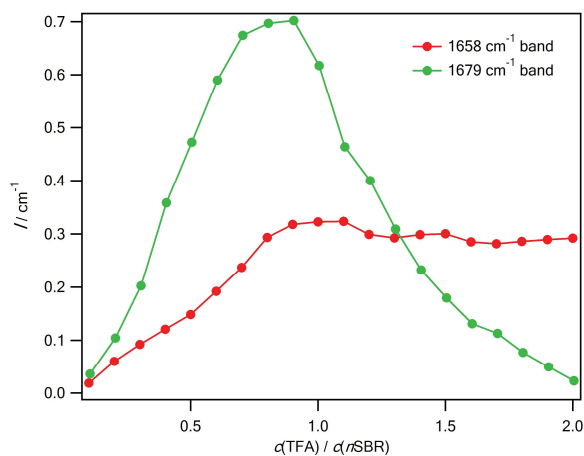


Figure 4. Intensity vs. $c(\text{TFA})/c(n\text{SBR})$ ratio for the components of the 1720–1640 cm^{-1} absorption envelope.

this region contains the $\nu(\text{C}=\text{N})$ and $\nu(\text{C}=\text{N}^+)$ stretches of *n*SBR and *n*SBR⁺, respectively. In the neutral *n*SBR molecule, the $\nu(\text{C}=\text{N})$ vibration is present as a weak band at 1652 cm^{-1} .⁵⁶ This oscillator, being directly involved in hydrogen bonding with TFA and consequent protonation, suffers changes in both $c(\text{TFA})/c(n\text{SBR})$ concentration regimes. As a matter of fact six distinct bands are evident in the 2D correlation maps. For $c(\text{TFA})/c(n\text{SBR}) < 1$ a wide absorption consisting of at least three components is centered at 1675 cm^{-1} . Figure 4 shows that the absorption at 1674 cm^{-1} increases for the ratio $c(\text{TFA})/c(n\text{SBR}) < 1$, while the further addition of TFA causes its decrease. The calculated $\nu(\text{C}=\text{N}^+)$ stretches of the two $[\text{nSBR}^+ \text{TFA}^-]$ conformers are located at 1677 and 1679 cm^{-1} . This indicates that the formation of the $\text{N}-\text{H}^+$ oscillator introduces considerable changes in the $\text{C}=\text{N}$ oscillator. From Figure 3 is evident that further addition of TFA ($c(\text{TFA})/c(n\text{SBR}) > 1$) leads to the formation of a well defined band peaking at 1656 cm^{-1} . The intensity of this band, however, remains constant (see Figure 4), implying that it is due to the protonated form of *n*SBR⁺ and it is also assigned to the $\nu(\text{C}=\text{NH}^+)$ vibration in $[\text{nSBR}^+ \text{TFA}^-]\text{TFA}$. DFT calculations show that the $\nu(\text{C}=\text{NH}^+)$ stretch vibration of $[\text{nSBR}^+ \text{TFA}^-]\text{TFA}$ is located at 1658 cm^{-1} , *i.e.* closer to the $\nu(\text{C}=\text{N})$ stretch in *n*SBR. Again, this con-

Table 1. Observed and calculated frequencies in the region 1500–1900 cm^{-1} . The harmonic $\nu(\text{C}=\text{NH}^+)$ stretching frequencies are scaled by 0.978. The $\nu(\text{CO})$ and $\nu(\text{OH}---\text{O})$ stretching frequencies are computed by solving Eq. 1 for four coupled normal modes

Obs. ^(a)	Calc.	Assignment
1805 w, sh	1801 ^(c)	$\nu(\text{OH}---\text{O})$ ^(c)
1785 m	1750 ^(c)	$\nu(\text{CO})$ ^(c)
1771 w, sh		
	1679 ^(d)	
1674 w	1677 ^(e)	$\nu(\text{C}=\text{NH}^+)$ ^(e)
1658 m	1660 ^(c)	$\nu(\text{C}=\text{NH}^+)$ ^(c)
	1567 ^(d)	
1608 s	1564 ^(e)	$\nu(\text{C}=\text{C})$ ^(c,d,e)
	1558 ^(c)	
	1602 ^(e)	
1563 ^(b) w, sh	1601 ^(d)	$\delta(\text{NH}^+) + \delta(\text{CH})$
	1593 ^(c)	
1559 ^(b) w, sh	1536 ^(d)	
1545 s	1531 ^(e)	$\delta(\text{NH}^+)$ ^(c,d,e)
1533 ^(b) w, sh	1520 ^(c)	

^(a) relative intensity of the bands: s – strong; m – medium; w – weak; sh – shoulder;

^(b) bands resolved by 2D IR analysis;

^(c) $[\text{nSBR}^+ \text{TFA}^-]\text{TFA}$;

^(d) $[\text{nSBR}^+ \text{TFA}^-]$ (lowest energy conformer);

^(e) $[\text{nSBR}^+ \text{TFA}^-]$ (higher energy conformer, local minimum).

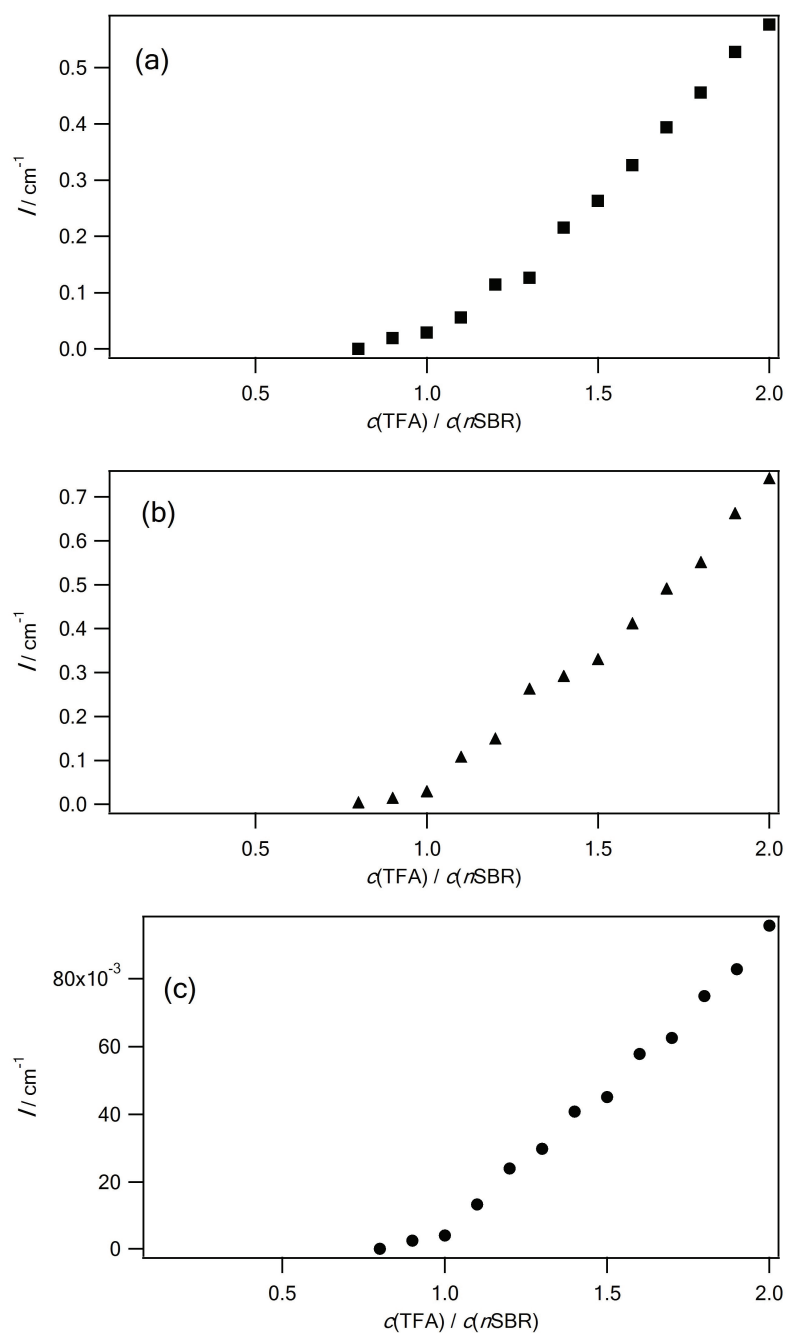


Figure 5. Intensity vs. $c(\text{TFA})/c(n\text{SBR})$ ratio for the bands (a) 1771 cm^{-1} ; (b) 1785 cm^{-1} and (c) 1805 cm^{-1} band, as obtained by fitting the 1900 – 1720 cm^{-1} region to three Voigt profiles.

firmly the weakening of the hydrogen bond in $[n\text{SBR}^+ \text{TFA}^-]\text{TFA}$.

In the $[n\text{SBR}^+ \text{TFA}^-]$ the hydrogen-bonded TFA molecule retains a relatively great freedom of rotation around the O–H---N hydrogen bond as testified by the existence of the two energetically close conformers shown in Figure 1 and reflected in a wide and complex absorption envelope of $\nu(\text{C}=\text{NH}^+)$. However, for $c(\text{TFA})/c(n\text{SBR}) > 1$ the formation of the second hydro-

gen bond causes a decrease of the rotational degree of freedom with a consequent fixed arrangement of the compound. In other words the decrease of rotational degrees of freedom makes the sample less heterogeneous.

(c) 1900–1720 cm^{-1} region

The formation of $[n\text{SBR}^+ \text{TFA}^-]\text{TFA}$ is characterized by strong changes of the absorption in the region between

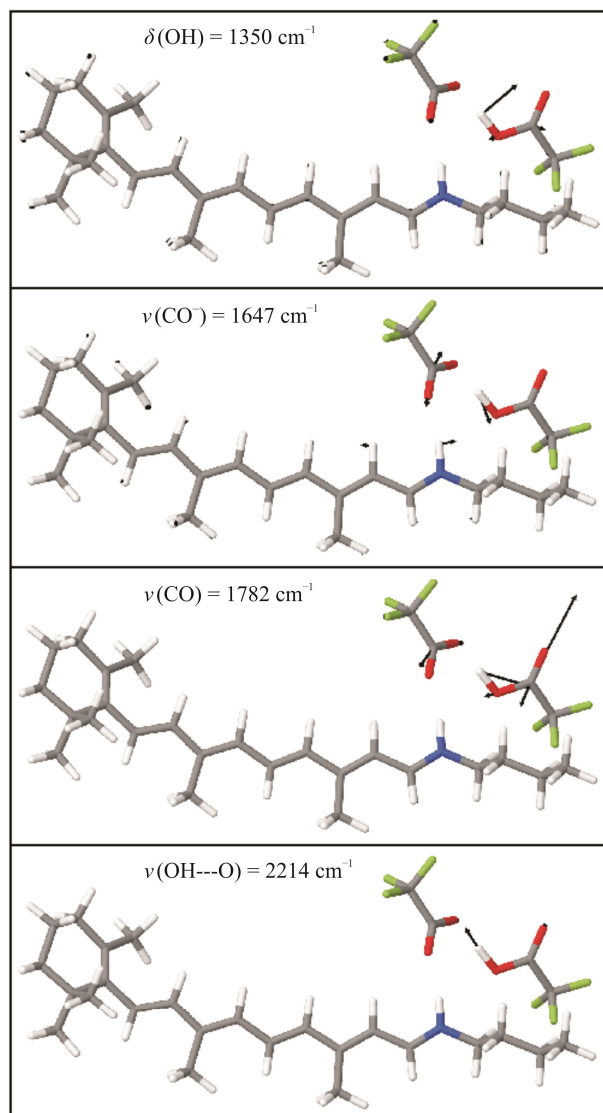


Figure 6. Normal mode displacement vectors and harmonic frequencies for the four modes which enter the 4D PES.

1787 and 1805 cm^{-1} . The 2D IR correlation maps show that this region consists of three bands. To obtain the concentration-dependent intensity of each component, the whole absorption is fitted to three Voigt profiles centered at 1771, 1785 and 1805 cm^{-1} . Figure 5 shows the intensity of each component as function of $c(\text{TFA})/c(n\text{SBR})$ ratio. It is evident that for $c(\text{TFA})/c(n\text{SBR}) < 1$ the intensity is negligible, while for $c(\text{TFA})/c(n\text{SBR}) > 1$ it increases linearly. For $[\text{nSBR}^+ \text{TFA}^-]\text{TFA}$, DFT calculations predict a harmonic $\nu(\text{OH}---\text{O})$ frequency of 2214.5 cm^{-1} , *i.e.* the harmonic frequency is upshifted by more than 400 cm^{-1} from the center of the observed band. We also note that at the B3LYP/TZVP level of theory the harmonic asymmetric $\nu(\text{OH}---\text{O})$ stretch vibration of the TFA dimer in dichloromethane is located at 3174 cm^{-1} . Hence, to assign the band at 1787–1805 cm^{-1} we need to compute the highly

Table 2. One-, three- and four-dimensional vibrational analysis of the ν_{OH} band of $[\text{nSBR}^+ \text{TFA}^-]\text{TFA}$ calculated at the B3LYP/TZVP level of theory

Dim.	Coordinate	Anharm. frequency (cm^{-1})
1D	δ_{COH}	1354
	ν_{CO^-}	1661
	ν_{CO}	1777
	ν_{OH}	1847
3D	δ_{COH}	1355
	ν_{CO^-}	1656
	ν_{CO}	1781
3D	δ_{COH}	1277
	ν_{CO^-}	1407
	ν_{OH}	1792
3D	δ_{COH}	1346
	ν_{CO}	1716
	ν_{OH}	1839
3D	ν_{CO^-}	1274
	ν_{CO}	1758
	ν_{OH}	1808
4D	δ_{COH}	1196
	ν_{CO^-}	1386
	ν_{CO}	1751
	ν_{OH}	1801

anharmonic frequency of $\nu(\text{OH}---\text{O})$ stretch vibration.³⁹

The normal mode displacement vectors of $\nu(\text{OH}---\text{O})$ (Q_4) and the three modes that most strongly couple to the $\nu(\text{OH}---\text{O})$ stretch are shown in Figure 6 together with the corresponding harmonic frequencies. The selected mode include the $\delta(\text{OH})$ (Q_1) bending vibration and two C=O stretching vibrations denoted $\nu(\text{CO}^-)$ (Q_2) and $\nu(\text{CO})$ (Q_3), respectively. As shown in Figure 6 both C=O vibrations have large contributions from the hydrogen bond stretching. The 4D potential energy surface was computed on a $Q_1 \times Q_2 \times Q_3 \times Q_4$ direct product grid with size $9 \times 9 \times 9 \times 21$. For the grid dimensions we used: -0.5 to 0.5 Å (Q_1), -0.3 to 0.3 Å (Q_2), -0.4 to 0.24 Å (Q_3) and -0.3 to 0.7 Å (Q_4).

In the 1D case the potential has been interpolated on 129 points, in the 3D case on a $31 \times 31 \times 31$ grid, and in the 4D case on a $21 \times 21 \times 21 \times 21$ grid. The results are

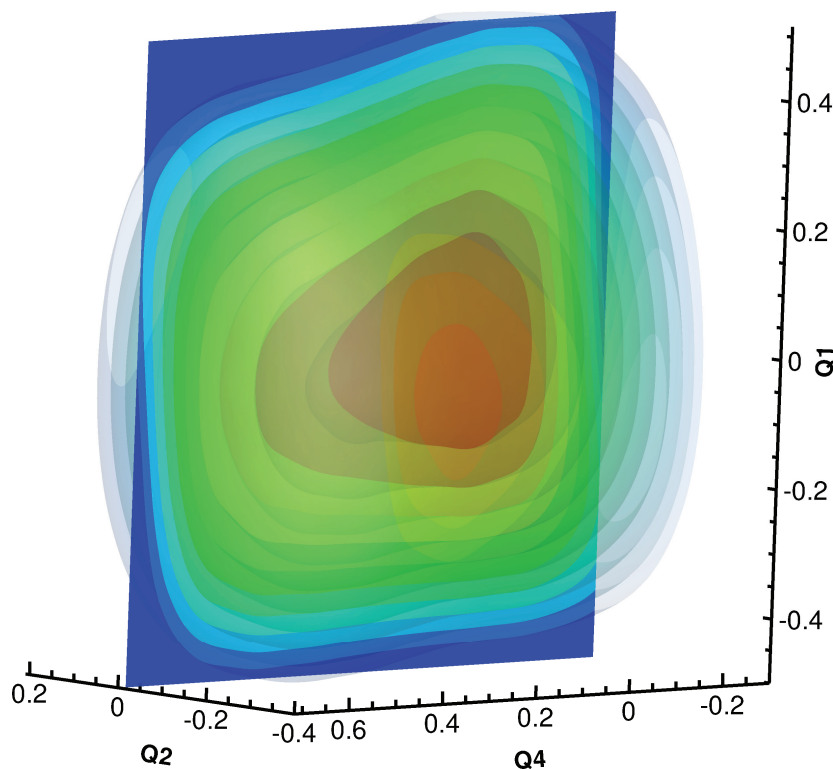


Figure 7. 3D cut of the 4D model PES for the hydrogen bond dynamics in $[n\text{SBR}^+ \text{TFA}^-]\text{TFA}$. The 3D PES includes the $\delta(\text{OH})$ bending vibration (Q_1), the C=O stretching vibration $\nu(\text{CO}^-)$ (Q_2) and the hydrogen bond stretching vibration $\nu(\text{OH}\cdots\text{O})$ (Q_4). The normal mode coordinates are in Å, the outermost energy contour is 3 eV and the contour spacing is 0.3 eV.

compiled in Table 2. It is apparent that already the 1D potential $\nu(\text{OH}\cdots\text{O})$ accounts for most of the anharmonicities as the $\nu(\text{OH}\cdots\text{O})$ frequency is shifted to 1847 cm^{-1} . The coupling to the selected modes leads to the further downshift of the band. The high anharmonicity of the interaction is visible in Figure 7 where the 3D cut, $V(Q_1, Q_2, Q_4)$ of the 4D model PES is shown. The $\nu(\text{OH}\cdots\text{O})$ frequencies computed for different 3D normal modes potentials indicate that the $\nu(\text{CO}^-)$ stretching vibration of TFA anion contributes to the strengthening of the hydrogen bond between the two TFA units, while the $\nu(\text{CO})$ vibration located on the TFA molecule weakens the bond. The two effects are balanced in the 4D case. Taking into account the reduced dimensionality of the PES, the computed $\nu(\text{OH})$ frequency of 1801 cm^{-1} finds very good agreement with the observed absorption band at $1787\text{--}1803 \text{ cm}^{-1}$. Furthermore, the calculation suggest to assign the broad band with center at 1767 cm^{-1} to the $\nu(\text{CO})$ stretch of the second TFA molecule.

CONCLUSION

In the present study, we have investigated the vibrational spectra of the protonated Schiff base of retinal in dichloromethane. The Schiff base was protonated by trifluoroacetic acid in the $0 < c(\text{TFA})/c(n\text{SBR}) < 2$ con-

centration ratio. We have shown that in the concentration range $c(\text{TFA})/c(n\text{SBR}) < 1$ an ionic pair $[n\text{SBR}^+ \text{TFA}^-]$ between the protonated Schiff base and the TFA counterion is formed. By increasing the $c(\text{TFA})/c(n\text{SBR})$ molar ratio, an aggregation with two hydrogen bonds, $[n\text{SBR}^+ \text{TFA}^-]\text{TFA}$, is formed. Taking into account that the photochemistry of the $n\text{SBR}^+$ in various solvents is studied using a 3-5 fold excess of TFA, $[n\text{SBR}^+ \text{TFA}^-]\text{TFA}$ should be the dominant photoactive species.

The unequivocal formation of the $[n\text{SBR}^+ \text{TFA}^-]\text{TFA}$ supports a view that electrostatic interactions with the corresponding counterion should play an important role in the photochemistry of $n\text{SBR}^+$ in solution. It remains to be checked in what extent the ultrafast dynamics and photoisomerization efficiency changes when the $c(\text{TFA})/c(n\text{SBR})$ concentration is exactly 1 and, thus, the formation of the $[n\text{SBR}^+ \text{TFA}^-]\text{TFA}$ complex is avoided.

From the methodological side we have shown that 2D correlation vibrational spectroscopy in combination with multidimensional quantum calculations is a powerful tool for studying complex hydrogen bonding interactions in solution.

Acknowledgements. This work has been supported by the Croatian MZOŠ projects 098-0352851-2921 and 098-2904-2927.

REFERENCES

- B. Honig, A. Warshel, and M. Karplus, *Acc. Chem. Res.* **8** (1975) 92–100.
- S. L. Dexheimer, Q. Wang, L. A. Peteanu, W. T. Pollard, R. A. Mathies, and C. V. Shank, *Chem. Phys. Lett.* **188** (1992) 6147–6158.
- J. Dobler, W. Zinth, W. Kaiser, and D. Oesterheld, *Chem. Phys. Lett.* **144** (1988) 215–220.
- M. Du and G. R. Fleming, *Biophys. Chem.* **48** (1993) 101–111.
- R. A. Mathies, C. H. Brito Cruz, W. T. Pollard, and C. V. Shank, *Science* **240** (1988) 777–779.
- H. J. Polland, M. A. Franz, W. Zinth, W. Kaiser, E. Kölling, and D. Oesterheld, *Biophys. J.* **49** (1986) 651–662.
- A. V. Sharkov, A. V. Pakulev, S. V. Chekalin, and Y. A. Matveet, *Biochim. Biophys. Acta* **808** (1985) 94–102.
- Q. Wang, R. W. Schoenlein, L. A. Peteanu, R. A. Mathies, and C. V. Shank, *Science* **266** (1994) 422–424.
- J. E. Kim, M. J. Tauber, and R. A. Mathies, *Biochemistry* **40** (2001) 13774–13778.
- J. E. Kim, M. J. Tauber, and R. Mathies, *Biophys. J.* **84** (2003) 2492–2501.
- N. Ferre and M. Olivucci, *J. Am. Chem. Soc.* **125** (2003) 6868–6869.
- A. Cembran, F. Bernardi, M. Olivucci, and M. Garavelli, *J. Am. Chem. Soc.* **126** (2004) 16018–16037.
- B. G. Levine and T. J. Martinez, *Ann. Rev. Phys. Chem.* **58** (2007) 613–634.
- S. Hayashi, E. Tajkhorshid, and K. Schulten, *Biophys. J.* **96** (2009) 403–416.
- D. Polli, A. Altoè, O. Weingart, and K. M. Spillane, C. Manzoni, D. Brida, G. Tomasello, G. Orlandi, P. Kukura, R. A. Mathies, M. Garavelli, and G. Cerullo, *Nature* **467** (2010) 440–443.
- R. W. Schoenlein, L. A. Peteanu, R. A. Mathies, and C. V. Shank, *Science* **254** (1991) 412–415.
- J. Herbst, K. Heynea, and R. Diller, *Science* **297** (2002) 822–825.
- U. Gether and B. K. Kobilka, *J. Biol. Chem.* **273** (1997) 17979–17982.
- R. S. Becker and K. Freedman, *J. Am. Chem. Soc.* **107** (1985) 1477–1485.
- K. Freedman and R. S. Becker, *J. Am. Chem. Soc.* **108** (1986) 1245–1251.
- Y. Koyama, K. Kubo, M. Komori, H. Yasuda, and Y. Mukai, *Photochem. Photobiol.* **54** (1991) 433–443.
- G. Zgrablić, S. Haacke, and M. Chergui, *J. Phys. Chem. B* **113** (2009) 4384–4393.
- T. Baasov and M. Sheves, *J. Am. Chem. Soc.* **107** (1985) 7524–7533.
- L. S. Lussier, C. Sandorfy, Le Thanh Hoa, and D. Vocelle, *J. Phys. Chem.* **91** (1987) 2282–2287.
- M. Han, B. S. DeDecker, and S. O. Smith, *Biophys. J.* **65** (1993) 899–906.
- J. G. Hu, R. G. Griffin, and J. Herzfeld, *J. Am. Chem. Soc.* **119** (1997) 9495–9498.
- P. Hamm, M. Zurek, T. Röschinger, H. Patzel, D. Oesterheld, and W. Zinth, *Chem. Phys. Lett.* **268** (1997) 180–186.
- D. Hadži and S. Bratos, *Vibrational Spectroscopy of the Hydrogen Bond*, in: P. Schuster, G. Zundel, and C. Sandorfy (Eds.), *The Hydrogen Bond – Recent Developments in Theory and Experiment*, Structure and spectroscopy, Vol II, North-Holland, Amsterdam, 1976, pp. 565–611.
- E. T. J. Nibbering, J. Dreyer, O. Kühn, J. Bredenbeck, P. Hamm, and T. Elsaesser, *Vibrational dynamics of hydrogen bonds*, in: L. Wöste and O. Kühn (Eds.), *Analysis and control of ultrafast photoinduced reactions*, Springer Heidelberg 2007, pp. 619–687.
- N. Biliškov, B. Kojić-Prodić, G. Mali, K. Molčanov, and J. Stare, *J. Phys. Chem. A* **115** (2011) 3154–3166.
- N. Biliškov and G. Baranović, *J. Phys. Chem. B* **112** (2008) 10638–10651.
- N. Biliškov and G. Baranović, *J. Mol. Liq.* **144** (2008) 155–162.
- J. Mavri and J. Grdadolnik, *J. Phys. Chem. A* **105** (2001) 2039–2044.
- I. Noda and Y. Ozaki, *Two-Dimensional Correlation Spectroscopy: Applications in Vibrational and Optical Spectroscopy*, 1st ed., Wiley, New York, 2002.
- Shipman, S. T. *et al.* Vibrational dynamics of carboxylic acid dimers in gas and dilute solution. *Phys. Chem. Chem. Phys.* **9**, 4572–4586 (2007).
- B. Kojić-Prodić, Z. Štefanić, and M. Žinić, *Croat. Chem. Acta* **77** (2004) 415–425.
- Z. Popović, G. Pavlović, V. Roje, N. Došlić, D. Matković-Čalagović and I. Leban, *Struct. Chem.* **15** (2004) 587–598.
- I. Matanović and N. Došlić, *J. Phys. Chem. A* **109** (2005) 4185–4194.
- M. Petković, J. Novak, and N. Došlić, *Chem. Phys. Lett.* **240** (2009) 248–252.
- J. Bertie, C. D. Keefe, and R.N. Jones, *Tables of Intensities for the Calibration of Infrared Spectroscopic Measurements in the Liquid Phase*, Blackwell Science, Carlton, 1995.
- <http://www.wavemetrics.com/>
- E. R. Malinowski, *Factor Analysis in Chemistry*, 3rd ed., Wiley, New York, 2002.
- Specfit Global Analysis System (v. 2.11, Spectrum Software Associates).
- M. J. Frisch, G. W. Trucks, H. B. Schlegel, G. E. Scuseria, M. A. Robb, J. R. Cheeseman, G. Scalmani, V. Barone, B. Mennucci, G. A. Petersson, H. Nakatsuji, M. Caricato, X. Li, H. P. Hratchian, A. F. Izmaylov, J. Bloino, G. Zheng, J. L. Sonnenberg, M. Hada, M. Ehara, K. Toyota, R. Fukuda, J. Hasegawa, M. Ishida, T. Nakajima, Y. Honda, O. Kitao, H. Nakai, T. Vreven, J. A. Montgomery, Jr., J. E. Peralta, F. Ogliaro, M. Bearpark, J. J. Heyd, E. Brothers, K. N. Kudin, V. N. Staroverov, R. Kobayashi, J. Normand, K. Raghavachari, A. Rendell, J. C. Burant, S. S. Iyengar, J. Tomasi, M. Cossi, N. Rega, J. M. Millam, M. Klene, J. E. Knox, J. B. Cross, V. Bakken, C. Adamo, J. Jaramillo, R. Gomperts, R. E. Stratmann, O. Yazyev, A. J. Austin, R. Cammi, C. Pomelli, J. W. Ochterski, R. L. Martin, K. Morokuma, V. G. Zakrzewski, G. A. Voth, P. Salvador, J. J. Dannenberg, S. Dapprich, A. D. Daniels, Ö. Farkas, J. B. Foresman, J. V. Ortiz, J. Cioslowski, and D. J. Fox, *Gaussian 09*, Gaussian, Inc., Wallingford CT, 2009.
- A. D. Becke, *J. Chem. Phys.* **98** (1993) 5648–5652.
- A. Schaefer, C. Huber, and R. Ahlrichs, *J. Chem. Phys.* **100** (1994) 5829–5835.
- W. Schneider and W. Thiel, *Chem. Phys. Lett.* **157** (1989) 367–373.
- M. Petković, *Chem. Phys.* **331** (2007) 438–446.
- C. C. Marston and G.G. Balint-Kurti, *J. Chem. Phys.* **91** (1989) 3571–3576.
- J. Stare and G. G. Balint-Kurti, *J. Phys. Chem. A* **107** (2003) 7204–7214.
- R. B. Lehoucq, D. Sorensen, and C. D. Yang, *ARPACK User's Guide: Solution of Large Scale Eigenvalue Problems with Implicitly Restarted Arnoldi Methods*, Rice University: Houston, 1997.
- A. Cooper, S. F. Dixon, M. A. Nutley, and J. L. Robb, *J. Am. Chem. Soc.* **109** (1987) 7254–7263.
- D. Lide, *CRC Handbook of Chemistry and Physics*, Internet Version 2005. CRC Press, Boca Raton, FL, 2005.
- R. I. Redington and K. C. Lin, *Spectrochim. Acta A* **27** (1971) 2445–2460.

55. I. Matanović, N. Došlić, and Z. Mihalić, *Chem. Phys.* **306** (2004) 201–207.
56. S. Smith, A. Myers, R. Mathies, J. Pardoen, C. Winkel, E. Vandenberg, and J. Lugtenburg, *Biophys. J.* **47** (1985) 653–664.
57. H. Gilson, B. Honig, A. Croteau, G. Zarrilli, and K. Nakanishi, *Biophys. J.* **53** (1988) 261–269.